Making Nonmagnetic Semiconductors Ferromagnetic

H. Ohno

REVIEW

Semiconductor devices generally take advantage of the charge of electrons, whereas magnetic materials are used for recording information involving electron spin. To make use of both charge and spin of electrons in semiconductors, a high concentration of magnetic elements can be introduced in nonmagnetic III-V semiconductors currently in use for devices. Low solubility of magnetic elements was overcome by low-temperature nonequilibrium molecular beam epitaxial growth, and ferromagnetic (Ga,Mn)As was realized. Magnetotransport measurements revealed that the magnetic transition temperature can be as high as 110 kelvin. The origin of the ferromagnetic interaction is discussed. Multilayer heterostructures including resonant tunneling diodes (RTDs) have also successfully been fabricated. The magnetic coupling between two ferromagnetic (Ga,Mn)As films separated by a nonmagnetic layer indicated the critical role of the holes in the magnetic coupling. The magnetic coupling in all semiconductor ferromagnetic/nonmagnetic layered structures, together with the possibility of spin filtering in RTDs, shows the potential of the present material system for exploring new physics and for developing new functionality toward future electronics.

The mass, charge, and spin of electrons in the solid state lay the foundation of the information technology we use today. Integrated circuits and high-frequency devices made of semiconductors, used for information processing and communications, have had great success using the charge of electrons in semiconductors. Mass storage of information—indispensable for information technology—is carried out by magnetic recording (hard disks, magnetic tapes, magneto-optical disks) using spin of electrons in ferromagnetic materials. It is then quite natural to ask if both the charge and spin of electrons can be used to further enhance the performance of devices. We may then be able to use the capability of mass storage and processing of information at the same time. Alternatively, we may be able to inject spin-polarized current into semiconductors to control the spin state of carriers, which may allow us to carry out qubit (quantum bit) operations required for quantum computing (*1*). However, there are good reasons why this has not yet been realized. The semiconductors used for devices and integrated circuits, such as silicon (Si) and gallium arsenide (GaAs), do not contain magnetic ions and are nonmagnetic (Fig. 1C), and their magnetic g factors are generally rather small. In order for there to be a useful difference in energy between the two possible electron spin orientations, the magnetic fields that would have to be applied are too high for everyday use. Moreover, the crystal structures of magnetic materials are usually quite different from that of the semiconductors used in electronics, which makes both materials incompatible with each other.

Ferromagnetism and semiconducting properties coexist in magnetic semiconductors, such as europium chalcogenides and semiconducting spinels that have a periodic array of magnetic elements (Fig. 1A) (*2*). In these magnetic semiconductors, which were extensively studied in the late 1960s to early 1970s, exchange interactions between the electrons in the semiconducting band and the localized electrons at the magnetic ions lead to a number of peculiar and interesting properties, such as a red shift of band gap when ferromagnetism sets in. Unfortunately, the crystal structure of such magnetic semiconductors is quite different from that of Si and GaAs; in addition, the crystal growth of these compounds is notoriously difficult. To obtain even a small, single crystal requires weeks of preparation and growth.

Making Nonmagnetic Semiconductors Magnetic

The usefulness of semiconductors resides in the ability to dope them with impurities to change their properties, usually to p- or n-type. This approach can be followed to introduce magnetic elements into nonmagnetic semiconductors to make them magnetic. This category of semiconductors, called diluted magnetic semiconductors (DMSs; Fig. 1B), are alloys of nonmagnetic semiconductor (Fig. 1C) and magnetic elements (*3*). Study of DMSs and their heterostructures have centered mostly on II-VI semiconductors, such as CdTe and ZnSe, in which the valence of the cations matches that of the common magnetic ions such as Mn. Although this phenomenon makes these DMSs relatively easy to prepare in bulk form as well as in thin epitaxial layers, II-VI–based DMSs have been difficult to dope to create p- and n-type, which made the material less attractive for applications. The magnetic interaction in II-VI DMSs is dominated by the antiferromagnetic exchange among the Mn spins, which results in the paramagnetic, antiferromagnetic, or spin-glass behavior of the material. It was not possible until very recently to make a II-VI DMS ferromagnetic at low temperature (<2 K) (*4*).

Ferromagnetic III-V Semiconductors

An approach compatible with the semiconductors used in present-day electronics is to make nonmagnetic III-V semiconductors magnetic, and even ferromagnetic, by introducing a high concentration of magnetic ions. The III-V semiconductors such as GaAs are already in use in a wide variety of electronic equipment in the form of electronic and optoelectronic devices, including cellular phones (microwave transistors), compact disks (semiconductor lasers), and in many other applications. Therefore, the introduction of magnetic III-V semiconductors opens up the possibility of using a variety of magnetic phenomena not present in conventional nonmagnetic III-V semiconductors in the optical and electrical devices already established.

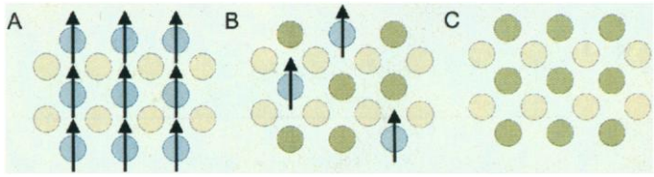

Fig. 1. Three types of semiconductors: **(A)** a magnetic semiconductor, in which a periodic array of magnetic element is present; **(B)** a diluted magnetic semiconductor, an alloy between nonmagnetic semiconductor and magnetic element; and **(C)** a nonmagnetic semiconductor, which contains no magnetic ions.

The author is with the Laboratory for Electronic Intelligent Systems, Research Institute of Electrical Communication, Tohoku University, Katahira 2-1-1, Sendai 980-8577, Japan. E-mail: ohno@riec.tohoku.ac.jp

The major obstacle in making III-V semiconductors magnetic has been the low solubility of magnetic elements (such as Mn) in the compounds. Because the magnetic effects are roughly proportional to the concentration of the magnetic ions, one would not expect a major change in properties with limited solubility of magnetic impurities, of the order of 10^{18} cm^{-3} or less. A breakthrough was made by using molecular beam epitaxy (MBE), a thin-film growth technique in vacuum that allows one to work far from equilibrium. When a high concentration of magnetic elements is introduced in excess of the solubility limit, formation of the second phase occurs if conditions are near equilibrium. However, when the crystal is grown at low temperature by MBE, there is not enough thermal energy available to form the second phase, and yet there still exists a local potential landscape that allows epitaxial growth of a single-crystal alloy. The effort to grow new III-V–based DMSs by low-temperature MBE was rewarded with successful epitaxial growth of uniform (In,Mn)As films on GaAs substrates in 1989 (*5*), where partial ferromagnetic order was found (*6*), and ferromagnetic (Ga,Mn)As in 1996 (*7*). In the remainder of this review, I describe the preparation and properties of ferromagnetic III-V semiconductors, with particular emphasis on (Ga,Mn)As, and what can be done with the heterostructures based on (Ga,Mn)As.

Molecular Beam Epitaxial Growth

(Ga,Mn)As films have been grown on semi-insulating (001) GaAs substrates in an MBE chamber equipped with solid sources of elemental Ga, Mn, Al, and As. Reflection high-energy electron diffraction (RHEED) patterns were used to monitor the surface reconstruction during growth, which was always carried out under As-stabilized conditions (excess of As). Either a GaAs buffer layer or an (Al,Ga)As buffer layer was then grown before growth of (Ga,Mn)As. For the GaAs buffer, after lowering the substrate temperature T_S to 250°C, a 100-nm GaAs layer was grown before the growth of 150- to 200-nm-thick (Ga,Mn)As, whereas for the (Al,Ga)As buffer, a high growth temperature of 600° to 700°C was maintained, and then T_S was lowered for (Ga,Mn)As growth. When the GaAs buffer layer growth was initiated at 250°C, the c(4×4) surface reconstruction pattern of GaAs changed to a (1×1) pattern. No change in the beam fluxes from the high-temperature growth of GaAs was made for this low-temperature GaAs growth. The (Ga,Mn)As growth was started by simply commencing the Mn beam during the low-temperature GaAs growth and keeping T_S constant at 250°C. No special precaution was taken at the start of (Ga,Mn)As growth. Typical growth rates were 0.6 μm/hour, with Mn concentration x in $(Ga_{1-x}Mn_x)As$ films up to 0.07. Although the properties of grown (Ga,Mn)As do depend on growth parameters such as As overpressure and T_S, as long as the established growth procedure was followed, the properties of (Ga,Mn)As films were reproducible; for example, for a given Mn concentration x, the ferromagnetic transition temperature T_C was always in the range of $2000x \pm 10$ K. The surface reconstruction of (Ga,Mn)As was (1×2) during and after growth. When the Mn flux or the substrate temperature, or both, were too high, a complex RHEED pattern appeared that indicated the appearance of the MnAs (NiAs structure) second phase on the surface. A schematic phase diagram of MBE growth is depicted in Fig. 2. Details of the growth can be found in (*7*–*9*).

Clear RHEED oscillations were observed at the initial stage of growth, which indicated two-dimensional layer-by-layer growth as opposed to island growth. One important finding is that GaAs grown at 250°C could still show very distinct oscillations. Although the oscillations were modified by the presence of Mn, which could act as a surfactant layer, clear oscillations were observed during low-temperature MBE of GaAs even in the growth chamber without a Mn cell. The systematic study on the RHEED oscillations of GaAs in the temperature range from 150° to 700°C was reported elsewhere (*10*).

Lattice Constant of (Ga,Mn)As

The lattice constants a of the (Ga,Mn)As layers (*7*) were determined by x-ray diffraction (XRD) as a function of x and are shown in Fig. 3 together with the results on (In,Mn)As (*5*). Asymmetric XRD on (115) reflection showed that the (Ga,Mn)As layers were fully strained, which indicates high-quality interface. This result was confirmed by the x-ray analysis of GaAs/(Ga,Mn)As superlattice structures (*11*). As can be seen from Fig. 3, a increases linearly with x following Vegard's law. The extrapolated lattice constants for zincblende MnAs (0.598 nm) are in good agreement with the MnAs lattice constant extrapolated from the (In,Mn)As side (0.601 nm). This lattice constant of hypothetical zincblende MnAs has been reproduced by a recent first-principle calculation (*12*). The agreement suggests that all of the Mn atoms were incorporated in the zincblende alloy, which was confirmed by

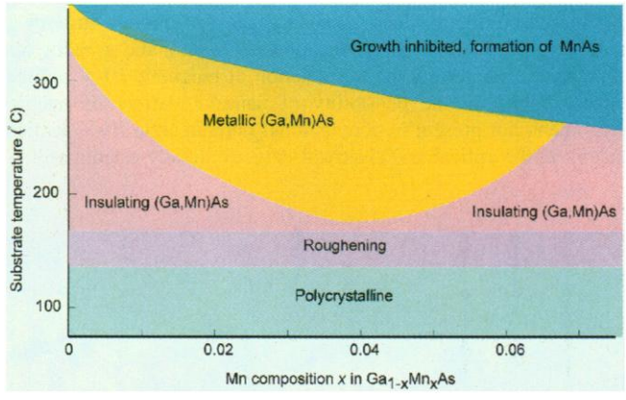

Fig. 2. Schematic phase diagram showing the relation between growth parameters (substrate temperature and Mn concentration) and the properties of (Ga,Mn)As grown by molecular beam epitaxy. The high concentration of Mn in excess of its solubility limit was introduced by nonequilibrium growth at low temperatures.

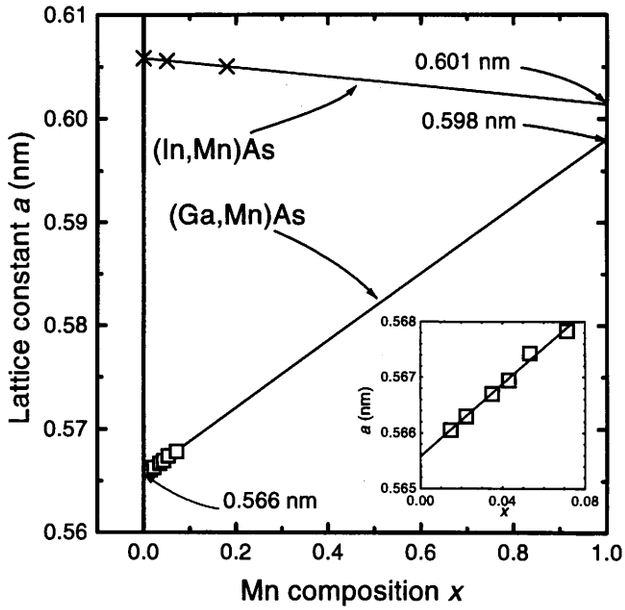

Fig. 3. Lattice constant a versus Mn composition x in $(Ga_{1-x}Mn_x)As$ films and in $(In_{1-x}Mn_x)As$ films. Extrapolation from the two end materials leads to the same point of 0.6 nm, which is believed to be the lattice constant of hypothetical zincblende MnAs.

Shioda *et al.* (*13*), who showed that Mn is indeed substitutionally incorporated into the Ga sublattice by extended x-ray absorption fine-structure measurement.

Magnetic Properties

Magnetization measurements with a SQUID (superconducting quantum interference device) magnetometer showed the presence of ferromagnetic order in the (Ga,Mn)As films at low temperatures (*7*). Sharp, square hysteresis loops, indicating a well-ordered ferromagnetic structure, appeared in the magnetization (M) versus magnetic field (B) curves when B was applied in the plane of the film. This sharp hysteresis was followed by a "paramagnetic" increase that appeared to follow a Brillouin function as B was further increased. This latter response seems to correlate with the transport properties of the films discussed below; the most metallic sample showed a negligibly small paramagnetic contribution, whereas in insulating samples, the paramagnetic contribution reached almost 50% of total saturation magnetization (*14*).

When the magnetic field was applied perpendicular to the sample surface, an elongated magnetization with little hysteresis was obtained, indicating that the easy-axis for magnetization was not perpendicular to the plane, but in the plane. This result is quite different from that observed in (001) (In,Mn)As, where the perpendicular direction was the only observed easy-axis (*15*). This difference may be explained by the magneto-elastic effect; the (In,Mn)As layers were under biaxial tensile strain, which makes the lattice spacing perpendicular to the surface smaller than the one in the plane, whereas the present (Ga,Mn)As layers were under compressive strain, which makes the in-plane lattice constant smaller than the perpendicular one. A perpendicular easy-axis was confirmed in the (Ga,Mn)As layer with biaxial tensile stress grown on an (In,Ga)As buffer layer, supporting the present explanation (*16*).

The low-temperature saturation magnetization, M_S, of the (Ga,Mn)As films was consistent with the spin of Mn $S = 5/2$, although it is difficult to determine S from these experiments alone because of the error involved in determining x and the nonuniformity of x over the sample.

Magnetotransport Properties

The dependence on temperature T (2 to 300 K) and magnetic field B (up to 7 T) of sheet resistance R_{sheet} and Hall resistance R_{Hall} of 150- to 200-nm (Ga,Mn)As layers were measured with a standard dc transport measurement setup. The temperature dependence of R_{sheet} in samples with intermediate Mn composition (x from 0.035 to 0.053) showed that they were on the metal side of the metal-insulator transition, whereas low- and high-x samples were on the insulator side. Although measurements were done on a number of metallic as well as insulating samples, in order to avoid complications arising from the localization effects, I concentrate here on the metallic samples, especially the one with $x = 0.053$; results for other metallic samples were essentially the same.

R_{Hall} can be expressed as

$$R_{Hall} = \frac{R_0}{d} B + \frac{R_s}{d} M \qquad (1)$$

where R_0 is the ordinary (normal) Hall coefficient, R_S is the anomalous Hall coefficient, d is the sample thickness, and M is the magnetization of the sample. R_S is proportional to R_{sheet} in the present samples [skew scattering (*17*)] and thus $R_S/d = cR_{sheet}$, where c is a constant. Because the anomalous Hall term is the dominant term up to room temperature, M of the sample can be determined from R_{Hall} [$M \sim (1/c)\, R_{Hall}/R_{sheet}$]. In order to determine the conduction type and the carrier concentration, the ordinary Hall coefficient was measured as the slope of the R_{Hall}-B curve at low temperature under high magnetic field, where M saturates.

The results of magnetotransport measurements on a sample with $x = 0.053$ are shown in Fig. 4, A and B. The T and B dependence of R_{Hall} reflects that of M, confirming the dominating contribution of the anomalous Hall effect. The sheet resistivity R_{sheet} first increases as T decreases with an increase of negative magnetoresistance (a decrease in resistance with increasing B). The zero-field resistivity peaks at around T_C and then decreases. The negative magnetoresistance also peaks at T_C. Using Arrott plots, in which $(R_{Hall}/R_{sheet})^2$ is plotted against $[B/(R_{Hall}/R_{sheet})]$ at each temperature to obtain a quantity that is proportional to the saturation magnetization M_S from the extrapolated intercept (Fig. 4C; M_S is zero when the intercept is at the origin), the T dependence of M_S and T_C can be determined; for the present

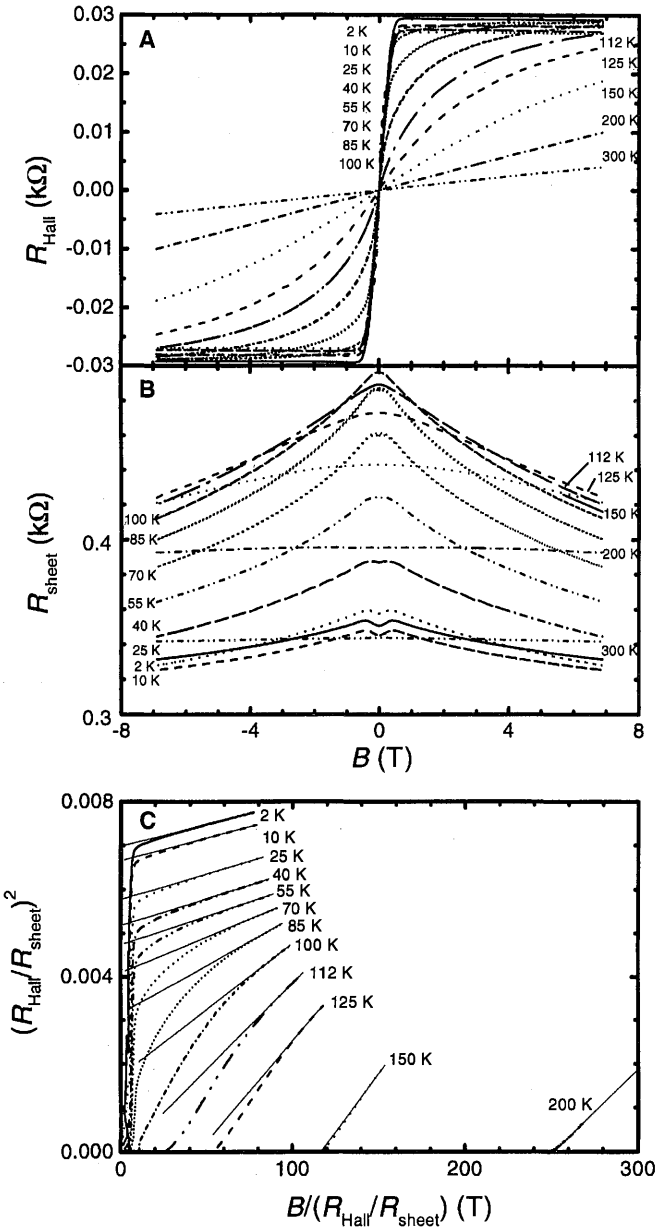

Fig. 4. Magnetic field dependence of (**A**) the Hall resistivity R_{Hall} and (**B**) the sheet resistivity R_{sheet} of (Ga,Mn)As ($x = 0.053$) with temperature as a parameter. Because the anomalous Hall term proportional to magnetization is dominant, R_{Hall} reflects the field and temperature dependence of magnetization perpendicular to the plane. From (A) and (B), and knowing that R_{Hall}/R_{sheet} is proportional to magnetization, the saturation magnetization and magnetic transition temperature can be determined with the Arrott plot shown in (**C**), which shows that the transition temperature is 110 K.

sample T_C = 110 K, which was the highest T_C for the studied samples. Note that R_{Hall}/R_{sheet} is proportional to M. The T dependence of M_S can be fitted with a standard Brillouin function, which seems to show that the ferromagnetism in (Ga,Mn)As can be understood in the framework of a mean-field theory. The paramagnetic Curie temperature θ was obtained from the T dependence of the inverse of the zero field slope of R_{Hall}/R_{sheet} (proportional to susceptibility χ). A straight line characteristic of the Curie-Weiss law was obtained. For all of the samples, θ was very close to T_C. The slope of R_{Hall}-B measured at 10 K revealed that the conduction type was p-type with a hole concentration of 1.0×10^{20} cm^{-3}.

The R_{sheet}-T curve showed a maximum at around T_C, which moved to higher T with increasing B. I have attributed this behavior of R_{sheet} to the scattering of carriers by magnetic fluctuation through exchange interactions (*18*), which has been observed in magnetic semiconductors (*19*), as opposed to metal-insulator transition proposed by Van Esch *et al.* (*20*). This interpretation is further supported by the high-temperature part of R_{sheet} being proportional to χT, as expected from the critical scattering. The observed negative magnetoresistance can be understood as the reduction of scattering by aligning the spins by B. Well above T_C, the B dependence of R_{sheet} can be fit to the following critical scattering resistivity formula

$$\rho_s = 2\pi^2 \frac{k_F}{ne^2} \frac{m^2\Gamma^2}{h^3} n_s[S(S+1) - \langle \mathbf{S} \rangle^2] \quad (2)$$

where k_F is the Fermi wavevector, n is the hole concentration, m is the effective mass, Γ is the p-d exchange, n_s is the Mn concentration, S = 5/2, $\langle \mathbf{S} \rangle$ is the average spin on Mn, e is the charge of an electron, and h is Planck's constant (*21*). By using the measured hole concentration and the effective mass of 0.5 m_0 (the free electron mass), the fit of Eq. 2 to experimental results for all of the metallic samples yields Γ = 150 ± 40 eV Å^3 or $N_0\beta \approx 3.3$ eV in terms of $N_0\beta$ commonly used to describe p-d interaction in DMSs. Typical p-d exchange ($N_0\beta$) in II-VI DMSs is about 1 eV. The origin of this large exchange is not clear at the moment; the effect of weak localization, which enhances the ferromagnetic interaction through electron-electron interaction, might have to be considered, and in the immediate vicinity of the metal-insulator transition, the description of spin-disorder scattering may have to be modified. Large p-d exchange in GaAs doped with Mn was reported by Szczytko *et al.* (*22*), who investigated magneto-optical properties. On the other hand, smaller exchange was inferred from photoemission experiments on (Ga,Mn)As (*23*).

Origin of Ferromagnetism

In the absence of holes, the magnetic interaction among Mn has been shown to be antiferromagnetic in n-type (In,Mn)As (*24*) and in fully carrier compensated (Ga,Mn)As (*25*). These results show that the ferromagnetic interaction is hole induced. I have examined whether the ferromagnetism fits into the framework of the Ruderman-Kittel-Kasuya-Yosida (RKKY) interaction, which was shown to be responsible for the carrier-induced ferromagnetism in a IV-VI compound (Pb,Sn,Mn)Te (*26*). T_C can be calculated from the exchange constant, and the hole concentration can be determined from the magnetotransport measurements. Although the result depends slightly on the cut-off length of the RKKY interaction, the calculated T_C was in good agreement with the experimentally determined T_C (*18*). Because of this quantitative agreement, I believe the RKKY interaction is most likely responsible for the appearance of ferromagnetism in (Ga,Mn)As. The oscillating nature of the RKKY interaction does not show up in the magnetism, presumably because of the low hole concentration. The sign of RKKY interaction is, in effect, only ferromagnetic because the first zero of the oscillation, beyond which the interaction changes its sign and becomes antiferromagnetic, occurs at a much greater distance (because of the low hole concentration) than the cut-off length of the interaction.

Ferromagnetism observed in insulating samples can probably be understood in the same framework, the carrier-mediated and RKKY-like interaction. In insulating samples close to the metal-insulator transition, the localization length is not extended over the sample size (millimeters), but is still quite long in comparison to the length scale of magnetic interactions (nanometers). Thus, the RKKY-like interaction can still be in effect in the insulating samples.

The understanding of the ferromagnetism of (Ga,Mn)As is not adequate, however. There are issues remaining to be studied such as to what extent the "pure" RKKY interaction is applicable to the present material system: It was pointed out (*4*), for example, that the behavior of the critical scattering may be qualitatively different when the spin-spin interaction is of long range (present case) as opposed to the short range interaction (magnetic semiconductors).

Spin-Dependent Resonant Tunneling

The fabrication of a ferromagnetic semiconductor compatible with the well-established GaAs-AlAs lattice–matched heterostructure system makes it possible to probe what can be achieved by combining semiconductor heterostructures and ferromagnetism. When semiconductors become ferromagnetic, spin splitting of the conduction as well as of the valence bands occurs because of s-d and p-d exchange interactions. I have chosen AlAs/GaAs/AlAs double-barrier resonant tunneling diode (RTD) structures with ferromagnetic p-type (Ga,Mn)As on one side and p-type GaAs on the other to see if holes of one spin type can be filtered using the energy difference of spin splitting in ferromagnetic (Ga,Mn)As (*27*).

The structure I studied consists of (from the surface side) 150-nm-thick ($Ga_{0.965}Mn_{0.035}$)As; 15-nm undoped GaAs spacer; 5-nm undoped AlAs barrier; 5-nm undoped GaAs quantum well; 5-nm undoped AlAs barrier; 5-nm undoped GaAs spacer; 150-nm Be-doped GaAs ($p = 5 \times 10^{17}$ cm^{-3}); 150-nm Be-doped GaAs ($p = 5 \times 10^{18}$ cm^{-3}); and p$^+$ GaAs substrates. All of the layers were grown at 650°C except for the last (Ga,Mn)As layer, which was grown at 250°C. A schematic zero-bias valence band diagram of the structures is depicted in the inset of Fig. 5. T_C of the (Ga,Mn)As layer is expected to be ~70 K.

As seen in Fig. 5, a total of six peaks have been observed in the dI/dV versus V curve of the present RTD. Each label in Fig. 5 indicates the resonance level in the GaAs well. When holes were injected from the (Ga,Mn)As side (positive bias), a spontaneous resonant peak splitting of the peak labeled HH2 was observed below T_C of (Ga,Mn)As without applying a magnetic field, as indicated in Fig. 5. The magnitude of the splitting is shown to be proportional to M_S calculated from the Brillouin function showing the origin of peak splitting as the spin splitting in the valence band of ferromagnetic (Ga,Mn)As. I therefore believe that the splitting observed in the I-V curves is due to the spin splitting of the valence band associated with the development of spontaneous magnetization in (Ga,Mn)As. The observation of splitting suggests that Fermi energies of the spin-split holes are greater than the energy separation of the spin-split bands and that the holes are not fully spin-polarized in (Ga,Mn)As. The reason why only HH2 shows a pronounced splitting is not understood at present. This RTD result shows the possibility of filtering one type of spin and injecting it into a nonmagnetic semiconductor by using an RTD energy filter combined with the energy difference of the spontaneous spin-split bands.

Interlayer Magnetic Interactions

Motivated by intense ongoing research on metallic multilayers (*28*), carrier-mediated magnetic interactions between two ferromagnetic (Ga,Mn)As layers separated by a nonmagnetic semiconducting layer was studied using (Ga,Mn)As-based heterostructures (*29*). The all-semiconductor ferromagnetic/nonmagnetic/ferromagnetic trilayer structures studied here consist of a 30-nm (Ga,Mn)As (x = 0.04) layer and a 30-nm (Ga,Mn)As (x = 0.02) layer separated by a nonmagnetic

(Al,Ga)As layer. The thickness of the intermediary layer was fixed to 10 monolayers, and the Al composition was varied (x_{Al} = 0.16 and 0.29), which varied the barrier in the valence band. Magnetic measurements (*M-B* curves, with *B* applied in the plane) revealed that the two layers were magnetically decoupled and that the *M-B* curve was a simple addition of the two individual *M-B* curves measured on separately grown samples for x_{Al} = 0.29. However, for x_{Al} = 0.16, the magnetization curve showed only one step, indicating that the two magnetic layers were now ferromagnetically coupled. The magnetic coupling between the two ferromagnetic (Ga,Mn)As films separated by a nonmagnetic GaAs layer was also shown to be a function of thickness of the intermediary GaAs layer. Both sets of results indicate the critical role of the holes in the intermediary layer on the magnetic coupling. This result is consistent with the RKKY interaction as the origin of the magnetic coupling in the present material system.

Prospects of Spin-Related Phenomena in Semiconductors

Driven by the thrust for faster and denser integrated circuits, semiconductor technology has experienced a continuous reduction in its working dimension, which now has reached a few tens of atomic spacing, if not less, at the most advanced structures. Spin of carriers become increasingly important in these small structures because the exchange interaction can become appreciable, even if the structure is made of nonmagnetic semiconductors (*30, 31*). In order to take advantage of this trend and use the spin degree of freedom in semiconductors, one has to be able to create, sustain, control, and detect the spin polarization of carriers. The most straightforward way to create spin polarization electrically is by "spin-injection," that is, by injection of spin-polarized carriers. To do this with ferromagnetic metal/semiconductor junctions has not been easy, presumably because of the presence of scattering at the Schottky barrier interface, although tunneling from a ferromagnetic metal through vacuum into a semiconductor was shown to provide a high degree of polarization (*32*) and, more recently, room-temperature operation of Si-based spin-valve transistors was demonstrated using spin-dependent transport over Schottky barriers (*33*). A very good interface between ferromagnet and semiconductor is critical for this application, and (Ga,Mn)As appears to be a promising candidate. How long the injected spin can exist depends on the spin relaxation time, which can be quite long in lightly doped nonmagnetic semiconductors (*34*). For control of spin, carrier-induced ferromagnetism might be used; by using field-effect to control the carrier density, ferromagnetism may be turned on and off. In fact, photo-generated carrier was recently used to induce ferromagnetism in (In,Mn)As (*35*). Detection requires spin-selective junction, which can again be provided by ferromagnetic materials with good interface to semiconductors.

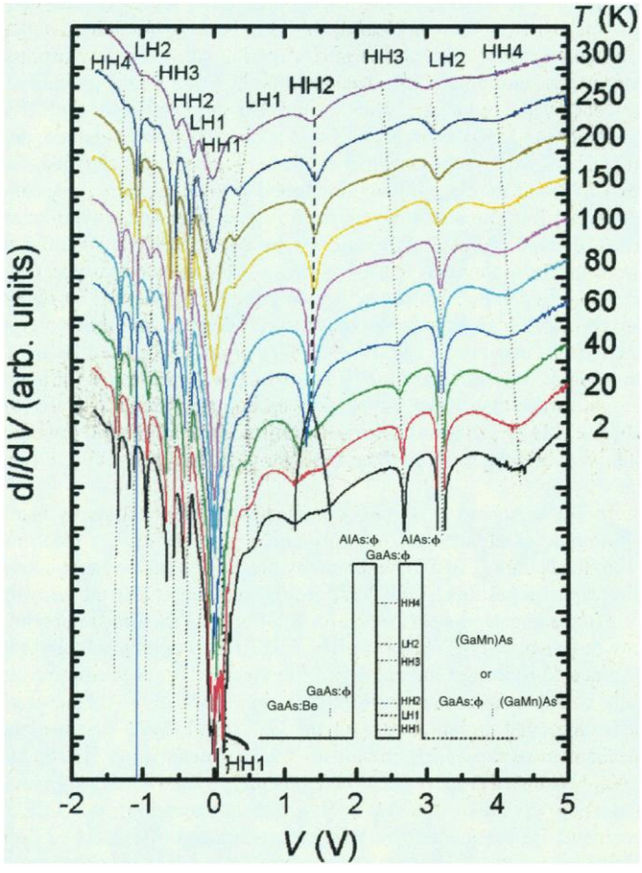

Fig. 5. Derivative of current (d*I*/d*V*) versus voltage (*V*) of a resonant tunneling diode with ferromagnetic (Ga,Mn)As emitter. The labeling indicates the relevant resonant state in the GaAs well. When holes are injected from the (Ga,Mn)As side (positive bias), a spontaneous splitting of resonant peak HH2 is observed below 80 K. The transition temperature of (Ga,Mn)As is expected to be 70 K. The splitting is attributed to spin splitting of (Ga,Mn)As valence band states.

Conclusion

The magnetic element Mn has been introduced into the nonmagnetic host-lattice of GaAs, widely used in semiconductor electronics, in excess of its solubility limit by low-temperature MBE. In this homogeneous alloy of GaAs and Mn—(Ga,Mn)As—Mn occupies Ga sites and provides magnetic moments as well as holes, which makes (Ga,Mn)As conducting. The hole-mediated ferromagnetic interaction results in ferromagnetism with a transition temperature as high as 110 K. (Ga,Mn)As can be grown on GaAs-related heterostructures coherently, which makes it possible to bring ferromagnetism and semiconductor heterostructure together. (Ga,Mn)As-based RTDs revealed the possibility of spin-filtering, and all-semiconductor ferromagnetic/nonmagnetic/ferromagnetic trilayer structures were used to investigate the interlayer magnetic interaction in semiconductors. The new III-V–based DMSs can thus be used to explore a new field in semiconductor physics and technology, where both semiconducting and magnetic properties play critical roles.

References and Notes

1. D. P. DiVincenzo, *Science* **270**, 255 (1995).
2. A. Mauger and C. Godart, *Phys. Rep.* **141**, 51 (1986).
3. J. K. Furdyna and J. Kossut, *Diluted Magnetic Semiconductors*, vol. 25 of *Semiconductor and Semimetals* (Academic Press, New York, 1988); T. Dietl, *Diluted Magnetic Semiconductors*, vol. 3B of *Handbook of Semiconductors*, (North-Holland, New York, 1994).
4. A. Haury *et al.*, *Phys. Rev. Lett.* **79**, 511 (1997).
5. H. Munekata *et al.*, *ibid.* **63**, 1849 (1989).
6. H. Ohno, H. Munekata, T. Penney, S. von Molnár, L. L. Chang, *ibid.* **68**, 2664 (1992).
7. H. Ohno *et al.*, *Appl. Phys. Lett.* **69**, 363 (1996).
8. F. Matsukura *et al.*, *Appl. Surf. Sci.* **113/114**, 178 (1997).
9. A. Shen *et al.*, *J. Cryst. Growth* **175/176**, 1069 (1997).
10. A. Shen, Y. Horikoshi, H. Ohno, S. P. Guo, *Appl. Phys. Lett.* **71**, 1540 (1997).
11. A. Shen *et al.*, *Jpn. J. Appl. Phys.* **36**, L73 (1997).
12. M. Shirai, T. Ogawa, I. Kitagawa, N. Suzuki, *J. Magn. Magn. Mater.* **177-181**, 1383 (1998).
13. R. Shioda, K. Ando, T. Hayashi, M. Tanaka, *Phys. Rev. B* **58**, 1100 (1998).
14. A. Oiwa *et al.*, *Solid State Commun.* **103**, 209 (1997).
15. H. Munekata, A. Zaslavsky, P. Fumagalli, R. J. Gambino, *Appl. Phys. Lett.* **63**, 2929 (1993).
16. H. Ohno *et al.*, *Proceedings of the 23rd International Conference on Physics of Semiconductors*, Berlin, 21 to 21 July 1996, M. Scheffler and R. Zimmermann, Eds. (World Scientific, Singapore, 1996), pp. 405–408.
17. C. L. Chien and C. W. Westgate, *The Hall Effect and Its Applications* (Plenum, New York, 1980), pp. 43–51.
18. F. Matsukura, H. Ohno, A. Shen, Y. Sugawara, *Phys. Rev. B* **57**, R2037 (1998).
19. S. von Molnár and T. Kasuya, *Phys. Rev. Lett.* **21**, 1757 (1968).
20. A. Van Esch *et al.*, *Phys. Rev. B* **56**, 13103 (1997).
21. T. Kasuya, *Prog. Theor. Phys.* **16**, 45 (1956).
22. J. Szczytko *et al.*, *Solid State Commun.* **99**, 927 (1996).

23. J. Okabayashi *et al.*, *Phys. Rev. B*, in press.
24. S. von Molnár, H. Munekata, H. Ohno, L. L. Chang, *J. Magn. Magn. Mater.* **93**, 356 (1991).
25. Y. Satoh, N. Inoue, Y. Nishikawa, J. Yoshino, *3rd Symposium on Physics and Application of Spin-Related Phenomena in Semiconductors*, Sendai, Japan, 17 to 18 November 1997, H. Ohno, Y. Oka, J. Yoshino, Eds., pp. 23–25.
26. T. Story, R. R. Galazka, R. B. Frankel, P. A. Wolff, *Phys. Rev. Lett.* **56**, 777 (1986).
27. H. Ohno *et al.*, *Appl. Phys. Lett.* **73**, 363 (1998).
28. B. Heinrich and J. A. C. Bland, Eds., *Ultrathin Magnetic Structures* (Springer-Verlag, Berlin, 1994), vol. 2, chap. 2, and references therein.
29. N. Akiba *et al.*, unpublished data.
30. S. Tarucha *et al.*, *Phys. Rev. Lett.* **77**, 3613 (1996).
31. D. Goldhaber-Gordon *et al.*, *Nature* **391**, 156 (1998).
32. S. F. Alvarado, *Phys. Rev. Lett.* **75**, 513 (1995).
33. D. J. Monsma, R. Vlutters, J. C. Lodder, *Science* **281**, 407 (1998).
34. J. M. Kikkawa and D. D. Awschalom, *Phys. Rev. Lett.* **80**, 4313 (1998).
35. S. Koshihara *et al.*, *ibid.* **78**, 4617 (1997).
36. I acknowledge F. Matsukura, A. Shen, N. Akiba, Y. Sugawara, T. Kuroiwa, T. Omiya, Y. Iye, S. Katsumoto, A. Oiwa, and T. Dietl for collaboration and discussion. Partially supported by a Grant-in-Aid for Scientific Research Priority Area "Spin Controlled Semiconductor Nanostructures" (09244103) from the Ministry of Education, Science, Sports and Culture, Japan, and by the "Research for the Future" program (JSPS-RFTF97P00202) from the Japan Society for the Promotion of Science.

The Roles of Structural Imperfections in InGaN-Based Blue Light–Emitting Diodes and Laser Diodes

Shuji Nakamura

REVIEW

High-efficiency light-emitting diodes emitting amber, green, blue, and ultraviolet light have been obtained through the use of an InGaN active layer instead of a GaN active layer. The localized energy states caused by In composition fluctuation in the InGaN active layer are related to the high efficiency of the InGaN-based emitting devices. The blue and green InGaN quantum-well structure light-emitting diodes with luminous efficiencies of 5 and 30 lumens per watt, respectively, can be made despite the large number of threading dislocations (1×10^8 to 1×10^{12} cm^{-2}). Epitaxially laterally overgrown GaN on sapphire reduces the number of threading dislocations originating from the interface of the GaN epilayer with the sapphire substrate. InGaN multi-quantum-well structure laser diodes formed on the GaN layer above the SiO_2 mask area can have a lifetime of more than 10,000 hours. Dislocations increase the threshold current density of the laser diodes.

The brightness and durability of light-emitting diodes (LEDs) make them ideal for displays, and semiconductor laser diodes (LDs) have been used in numerous device applications from optical communications systems to compact disk (CD) players. These applications have been limited, however, by the lack of materials that can emit blue light efficiently. Full-color displays, for example, require at least three primary colors, usually red, green, and blue, to produce any visible color. Such a combination is also needed to make a white light–emitting device that would be more durable and consume less power than conventional incandescent bulbs or fluorescent lamps. The shorter wavelength means that the light can be focused more sharply, which would increase the storage capacity of magnetic and optical disks. Digital versatile disks (DVDs), which came onto the market in 1996, rely on red aluminum indium gallium phosphide (AlInGaP) semiconductor lasers and have a data capacity of about 4.7 gigabytes (Gbytes), compared to 0.65 Gbytes for compact disks. By moving to violet wavelengths emitted by III-V nitride-based semiconductors, the capacity could be increased to 15 Gbytes. The violet III-V nitride-based LDs could also improve the performance of laser printers and undersea optical communications. Such III-V nitride-based semiconductors have a direct band gap that is suitable for blue light–emitting devices. The band gap energy of aluminum gallium indium nitride (AlGaInN) varies between 6.2 and 2.0 eV, depending on its composition, at room temperature (RT). Thus, by using these semiconductors, red- to ultraviolet (UV)-emitting devices can be fabricated.

The first breakthrough for III-V nitride-based semiconductors was the use of AlN (*1*, *2*) or GaN (*3*, *4*) nucleation layers for the GaN growth. By using these nucleation layers, it became possible to obtain high-quality GaN films with a mirrorlike flat surface, a low residual carrier concentration, high carrier mobilities, and a strong photoluminescence (PL) intensity. The second big breakthrough for III-V nitride-based LEDs and LDs was that *p*-type GaN was obtained, and the reasons why *p*-type GaN had not been obtained were clarified. For the LEDs and LDs, a *p-n* junction is used to inject carriers (holes and electrons) into the active layers from *p*-type layer and *n*-type layer. Thus, control of both *p*-type and *n*-type conductivity is required to fabricate those devices. It was relatively easy to make *n*-type GaN from the beginning. However, it was virtually impossible to obtain *p*-type GaN films for many years (*5*, *6*). The unavailability of *p*-type GaN films had prevented III-V nitrides from being used in light-emitting devices, such as blue LEDs and LDs. Since the 1970s, many people had tried to make *p*-type GaN by doping with Zn (*7*), Be (*8*), Mg (*9*), Cd (*10*), and similar metals as an acceptor impurity. However, unknown reasons prevented the formation of a low-resistivity, *p*-type GaN by doping.

In 1989, Amano *et al.* (*11*) obtained *p*-type GaN films by using Mg-doping as an acceptor impurity and a post low-energy electron-beam irradiation (LEEBI) treatment by means of metal organic chemical vapor deposition (MOCVD) growth method. After the growth, LEEBI treatment was performed for Mg-doped GaN films to obtain a low-resistivity *p*-type GaN film. The LEEBI treatment was thought to displace Mg through the energy of the electron beam irradiation. In spite of this achievement in forming *p*-type GaN, only Amano *et al.* had succeeded in obtaining *p*-type GaN until 1992 because the mechanism of the LEEBI treatment was not understood exactly. In 1992, Nakamura *et al.* (*12*, *13*) obtained *p*-type GaN films by thermal annealing of GaN films in a N_2-ambient instead of the LEEBI treatment. Before thermal annealing, the resistivity of Mg-doped GaN films was $\sim 1 \times 10^6$ ohm·cm. After thermal annealing at temperatures above 700°C, the resistivity dropped to 2 ohm·cm (*12*). Low-resistivity *p*-type GaN films, which were obtained by N_2-ambient thermal annealing, showed a resistivity as high as 1×10^6 ohm·cm after NH_3-ambient thermal annealing at temperatures above 600°C (*13*).They proposed that atomic hydrogen produced by NH_3 dissociation at temperatures above 400°C was related to the acceptor com-

The author is in the Department of Research and Development, Nichia Chemical Industries, 491 Oka, Kaminaka, Anan, Tokushima 774, Japan. E-mail: shuji@nichia.co.jp